Journal of Engineering Technology and Applied Physics

An Improved DC-DC Boost Converter for Energy Harvesting

Florence Chiao Mei Choong* and Yeo Yin May
School of Engineering and Physical Sciences, Heriot-Watt University, Putrajaya, Malaysia.
**Corresponding author:* f.choong@hw.ac.uk, *ORCiD:* 0000-0002-6958-8725
https://doi.org/10.33093/jetap.2023.5.2.8
Manuscript Received: 12 February 2023, Accepted: 9 May 2023, Published: 15 September 2023

***Abstract* — A novel dual-input DC-DC boost converter that can perform the integration of harvested energy from solar and vibrational input energy sources is proposed. Firstly, the background of a hybrid energy system that relates to multi-input DC-DC converters is discussed, and the limitations of the current designs of power converter ICs are highlighted. A detailed design analysis of the proposed converter was done to justify its performance. A current and voltage stress analysis has been performed to ensure suitable switching devices are selected for the converter. Two different power control strategies are proposed for the DIDCB converter to manage output voltage during source and load-side disturbances. Performance analysis of the circuit is carried out using MATLAB Simulink software. Different duty ratios for power switches in the converter were tested to determine the maximum boost ratio and the highest efficiency that can be achieved by the converter. To demonstrate the feasibility of the proposed converter, the performance of the converter is compared with existing converter topologies. The proposed converter achieved a high efficiency of 99.4%, had less fluctuation in the output voltage, and had reduced overshoot. In addition, the proposed converter demonstrated a simpler configuration and required fewer component counts, which helped reduce the cost and size of the system.**

Keywords* — *Boost converter, Hybrid energy system, Dual-input DC-DC boost converter, Energy harvesting

I. INTRODUCTION

Non-renewable sources, such as oil, uranium, coal, and natural gas, are some of the main reasons for environmental pollution. They are known as the largest contributors to greenhouse gas emissions, which lead to global warming. Hence, harvesting energy like solar, geothermal, tidal, wind, and fuel cells from the environment has become a viable option to replace current power supplies used for energy-constrained embedded systems [1]. Renewable energy sources are clean, abundant in nature, and pose less potential harm to the environment. However, renewable sources are often dependent on climate conditions that are inconsistent and unforeseeable. This makes it difficult to produce the same amount of electricity when compared to that generated from conventional energy sources.

Therefore, many researchers are working towards a hybrid energy system (HES), which uses multiple renewable energy sources. These systems can accommodate the different voltage-current (V-I) characteristics of renewable energy sources and storage with the use of power converter ICs to integrate these sources [2]. Hence, HES provides more flexibility in terms of choices, availability of energy sources, and enhancing the reliability of the system.

Multi-input DC-DC converters (MIDC) can be categorised into isolated and non-isolated topologies [3–7]. An isolated power converter is designed to prevent direct current flow from input to output by separating the circuit into two sections, which is usually achieved by using a transformer. This topology can provide benefits such as breaking ground loops and ensuring safety compliance in an application by having input and output return to their own independent ground. However, multi-winding transformer-based topologies are complex, bulky, and costly to implement. Khaligh *et al.* [3] introduced a multi-input bidirectional dc-dc topology without any transformer to provide the same benefits and a positive output voltage. It can operate in a bidirectional manner without the need for additional converters and can work in boost, buck, and buck-boost modes. However, one of the drawbacks is that the topology can only have one input voltage-transfer energy into the load at a time.

Published by MMU PRESS. URL: https://journals.mmupress.com/index.php/jetap/index

For solar electric systems, a single-input, dual-output DC-DC boost converter that converts unregulated DC to controlled DC was proposed [4]. A voltage regulator is applied in this circuit to always maintain a 12 V input voltage. Another work proposed a three-input dc-dc boost converter, where the proposed structure utilises only four independently controlled power switches, with each having a different duty ratio [5]. However, this design can only be used for certain input sources, which are fuel cells, batteries, and PV sources. Similar designs were introduced for single-stage, multi-input DC-DC/AC boost converters [6–7]. Both designs can directly boost low-level DC input voltage to high-level output voltage without the use of any output filter.

On the other hand, a non-isolated power converter is a single circuit where the current can flow directly from input to output and vice versa. A non-isolated multi-input, multi-output (MIMO) dc-dc boost converter for electric vehicle applications was presented in [8]. It uses a multilevel inverter to reduce voltage harmonics, which leads to a reduction in torque ripple in induction motors. Another work developed a new structure for MIMO dc-dc boost converters that is applicable for hybrid energy systems [9]. It has the advantages of continuous input current and the possibility of using energy sources with different V-I characteristics. However, the design becomes more complex as the number of DC voltage sources increases. A multi-source energy harvesting power management system with a DC-DC buck-boost converter with an 87% efficiency level was developed [10]. Detailed modelling and experimental verification of a bidirectional DC/DC boost converter-inverter as a driver for a DC motor have been examined in [11].

Chen *et al.* [12] proposed a PV and piezoelectric energy harvesting system based on the topology of the buck-boost converter. This converter consists of a maximum-power point tracking (MPPT), a current sensing circuit with slope compensation, control circuits, a rectifier, a gate driver, a zero-current detector (ZCD), an input compensator and an output compensator [12]. For a wider power range, a new MIMO dc-dc converter was presented in [13] with a high step-up capability. It can use different input sources with various voltage levels and powers. In addition, a novel topology for the extendable high-step-up multi-input, single-output dc-dc converter was proposed in [14]. Although the many input stages make the design bulky, this converter has simple control of each duty cycle and low-voltage stress across semiconductors.

Recent works have proposed a single-input, multiple-output (SIMO) converter using coupled inductors that includes buck operation [15-17]. However, the use of these converters is restricted to low-power applications. In addition, SIMO-based converters suffer from cross-regulation [18].

Most conventional schemes that use parallel-connected single-input DC-DC power converters lead to losses in system efficiency, substantial complexity in control strategies, and increased cost and size of the system [19, 20]. Therefore, the idea of MIDC has been proposed to overcome the drawbacks of conventional schemes. One of the main attractive features of MIDC is the lower count of active and passive components, which can greatly reduce the cost and size of the system. However, work related to a dual-input DC-DC boost converter that is suitable to perform integration of harvested energy, specifically from solar and vibrational energy power sources, has been limited in recent years. Therefore, the contribution of this paper is the design of a dual-input DC-DC boost converter based on a lower count of active and passive components, which will greatly reduce the cost and size of the system while improving system efficiency. A suitable power control strategy based on average current mode (ACM) control was designed to regulate output voltage during source-side and load-side disturbances of the circuit.

II. METHODOLOGY

Figure 1 shows the block diagram of the proposed solar and vibration-based electric system. The dual-input DC-DC boost converter (DIDCB), which is the focus of this paper, aims to harvest energy from rechargeable batteries, which are supplied by a photovoltaic thermal (PV/T) module and a piezoelectric transducer (PZT). The PV system consists of three elements: the PV/T module, the solar charge controller, and the rechargeable battery. When sunlight hits the surface of the PV/T module, this causes electrons from the solar cells to loosen up and generate a flow of electric current. The electrical energy that flows from the PV/T module is regulated by the solar charge controller to protect the battery from overcharging. A 12V rechargeable battery stores this energy before sending it to the DIDCB as an input source.

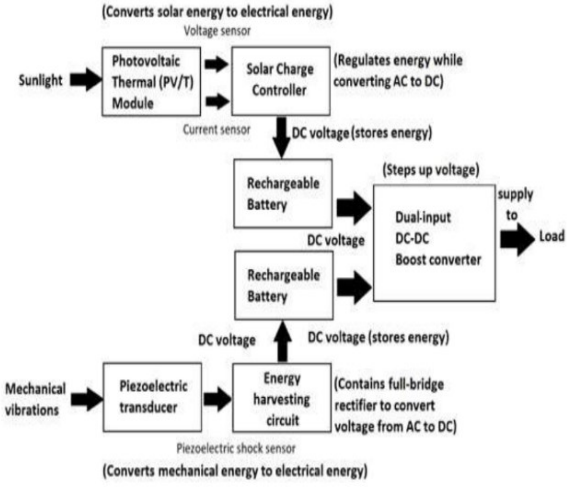

Fig. 1. Block diagram of solar and vibration-based electric system.

A. DIDCB Converter

Figure 2 shows the circuit design for the proposed DIDCB converter. Rechargeable batteries V_1 and V_2 represent the input sources in this converter. They are constantly charged by energy generated from the PV/T module and PZT, respectively. For unidirectional operation of this converter, only two diodes (D_1 and D_2), two power switches (S_1 and S_2), a capacitor C and an inductor L were considered, while R represents the load.

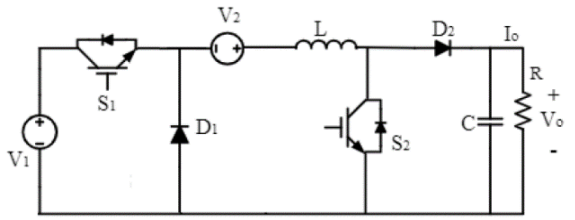

Fig. 2. Proposed DIDCB converter for unidirectional operation.

Switches S_1 and S_2 are used to control the series and parallel operations of V_1 and V_2. All possible working states for this converter are reflected in Fig. 3. Based on the switching strategy for switches S_1 and S_2, the DIDCB converter has four operating states, as shown in Fig. 3 (a) - (d).

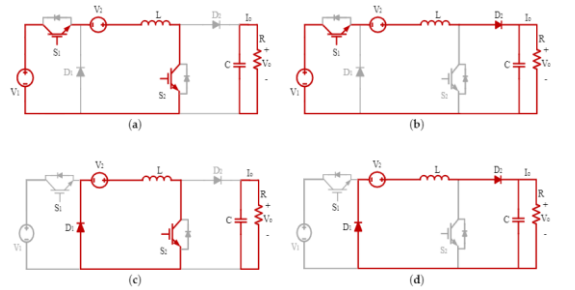

Fig. 3. Different working states of proposed converter for unidirectional operation: (a) Inductor charged by both $\boldsymbol{V_1}$ and $\boldsymbol{V_2}$, (b) Inductor discharges to load, (c) Inductor charged by $\boldsymbol{V_2}$ and (d) Inductor discharges to load.

There are four possible working states for this converter as follows:

State 1: The inductor is charged by both sources V_1 and V_2 when switches S_1 and S_2 are turned ON for a certain time. Then the capacitor supplies energy to the load.

State 2: Switch S_2 is turned OFF while switch S_1 is still ON. The inductor discharges energy to the load through diode D_2.

State 3: Switch S_1 is turned OFF while switch S_2 is turned ON. Here, the inductor is charged by source V_2, and the capacitor supplies energy to the load.

State 4: Both switches S_1 and S_2 are turned OFF. Diodes D_1 and D_2 are in forward-biased condition. The load is provided with stored energy discharged from the inductor through diodes D_1 and D_2.

Figure 4 shows the key waveforms of the DIDCB converter based on Fig. 3. Working states in Fig. 3(a) and Fig. 3(b) were considered, as the combination of these two working states provided a higher output voltage and boost ratio for the proposed converter. The output characteristics of the DIDCB converter are determined by several important performance parameters. The current through the inductor I_L is given in Eq. (1).

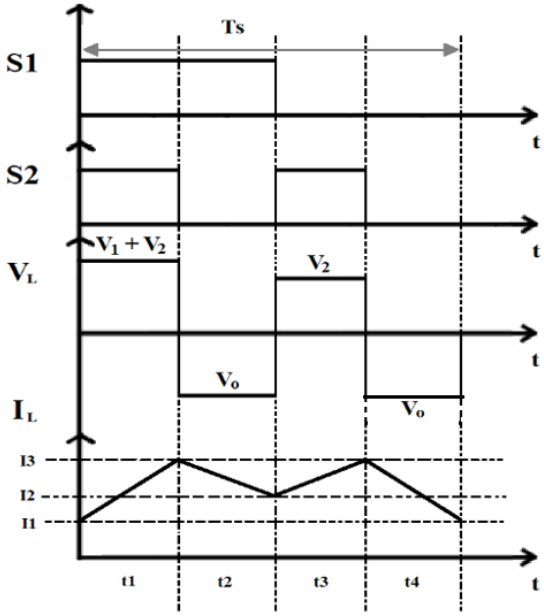

Fig. 4. Key waveforms of DIDCB converter.

$$I_L = \frac{1}{L}\int_0^t (V_1 + V_2)\,dt + I_{L(\min)} \quad (1)$$

, where

V_1 = input source 1 voltage, V

V_2 = input source 2 voltage, V

L = inductor value, H

$I_{L(min)}$ = minimum inductor current, A

Equations (2) and (3) show the expressions for the inductor current when power switch S_2 operates in ON mode and OFF mode, respectively.

$$I_{L(\max)} = \frac{(V_1+V_2)(d_{S2}T_S)}{L} + I_{L(\min)} \quad (2)$$

$$I_{L(\min)} = \frac{(V_1+V_2-V_o)(1-d_{S2})(T_S)}{L} + I_{L(\max)} \quad (3)$$

, where

$I_{L(\max)}$ = maximum inductor current, A

V_o = output voltage, V

d_{S2} = duty ratio of power switch S_2

T_s = switching period, s

Equation (4) gives the output voltage V_o. The duty ratio d_{S2} can be calculated using Eq. (5).

$$V_o = \frac{(V_1+V_2)}{1-d_{S2}} \quad (4)$$

$$d_{S2} = \frac{t_{on}}{T_s} \quad (5)$$

, where

t_{on} = ON time of power switch S_2, s

The DIDCB converter is assumed to be a lossless system. Therefore, the input power is equal to the output power as given in Eq. (6).

$$(V_1 + V_2)I_i = V_o I_o \quad (6)$$

, where

I_i = input current, A

I_o = output current, A

The efficiency of the converter is calculated based on Eq. (7).

$$\eta = \frac{P_{output}}{P_{input}} \times 100\% \quad (7)$$

B. Control Strategy for DIDCB Converter

Suitable control mechanisms to resolve the power management problems in a multi-input DC-DC converter were proposed by considering the steady-state and dynamic behaviour of the input sources used, as well as the power extracted from each energy source. ACM control is implemented as the control strategy for the DIDCB converter to manage the output voltage during source and load side disturbances. There are two approaches available for ACM: load-side control and source-side control. During load-side control, the inductor current is directly used to regulate the load voltage. On the other hand, inductor current in source-side control is indirectly regulated to control the load voltage based on the source current. Two different power control strategies based on source-side control were proposed. Both control strategies use proportional-integral (PI) controllers for both the voltage controller and current controller, as they provide better stability to the system, good transient response, ease of implementation, and reduced steady-state error.

Figure 5 shows the implementation of control strategy 1. Higher efficiency can be obtained when power switch S_1 is always turned ON. Hence, this converter considers only the regulation of the duty ratio for power switch S_2 to control the output voltage. At first, the output voltage is compared with the desired output voltage value to obtain the corresponding voltage error. The error is then provided to a voltage controller, which gives the value of the reference current, I_{ref}. Then, the reference current is compared with the actual inductor current to acquire the corresponding current error. Finally, this error is fed into the PWM generator to produce PWM pulses to control the duty cycle of the power switch S_2 for regulating the output voltage.

Figure 6 illustrates the second control strategy proposed for the DIDCB converter. It improves on the design of the first control strategy by adding the current controller and saturation block. The desired output voltage value is first compared with the output voltage measured from the load to acquire the corresponding voltage error. The error is fed into the voltage controller. The output of the voltage controller is known as the reference current, I_{ref}. Then, it is compared with the actual inductor current value to obtain the corresponding current error. The current controller tunes the values of the current error before passing it to a saturation block. Upper and lower limits for the duty ratio of power switch S_2 are defined in the saturation block for better output regulation. Finally, pulses are produced by the PWM generator based on the output from the saturation block. Hence, even when there are source-side and load-side disturbances in the DIDCB converter, the duty ratio of power switch S_2 can be easily controlled by using the proposed control strategy.

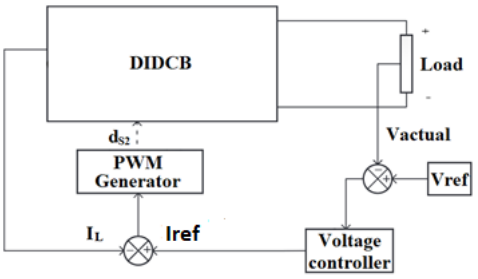

Fig. 5. Control Strategy 1.

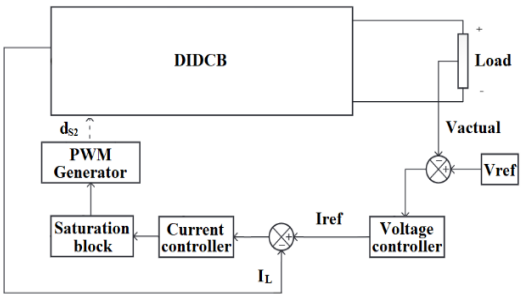

Fig. 6. Control Strategy 2.

III. RESULTS AND DISCUSSION

The circuit is simulated using the design parameters given in Table I. The system identification toolbox and control system toolbox, which consist of proportional-integral-derivative (PID) tuner applications in MATLAB Simulink software, were used for PI tuning of the voltage and current controllers.

Table I: Design parameters for DIDCB converter.

Source 1 (V)	Source 2 (V)	Duty ratio		Inductor L (mH)	Capacitor C (μF)	Switching frequency f_s (kHz)	Load Resistance R (Ω)	Output voltage (V)
		d_1	d_2					
70	90	0.5	0.5	10	4.7	20	64	238 to 260

The simulation waveforms for the output and inductor voltages are illustrated in Fig. 7. The simulation waveforms for the output and inductor currents are given in Fig. 8. Figure 9 shows how the

output voltage varies with the changes in the duty ratio, ranging from 0.5 to 0.9, while the value of d_1 is equal to the value of d_2. Due to the output voltage, $V_o = V_o = \frac{(V_1+V_2)}{1-d_2}$, the output voltage increases when the duty ratio increases.

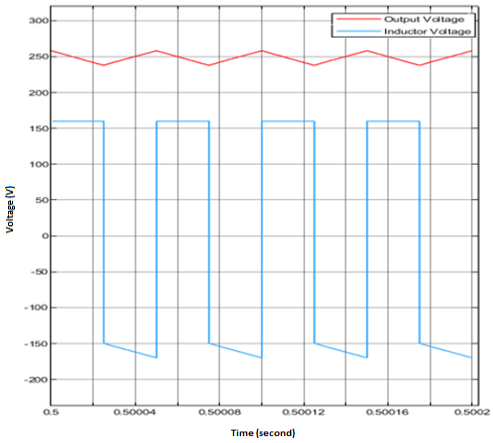

Fig. 7. Simulation waveforms for output and inductor voltages of DIDCB converter.

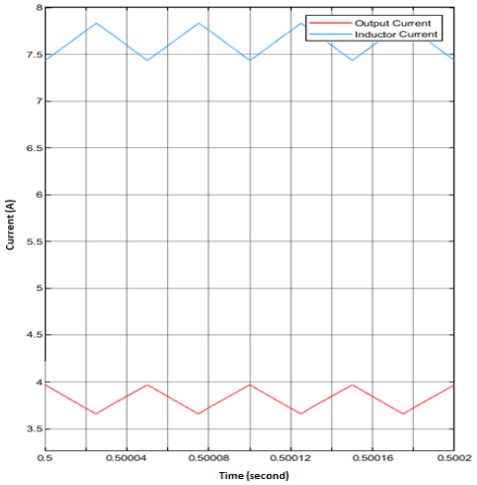

Fig. 8. Simulation waveforms for output and inductor currents of DIDCB converter.

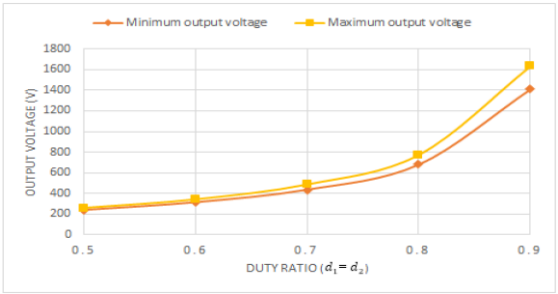

Fig. 9. Output voltage variation with different values of duty ratios.

The converter design incorporating the modified control strategy from the literature is shown in Fig. 10. The duty ratio dS_2 for power switch S_2 is modulated by the strategy for regulating the output voltage. The desired output is set to 264 V. The proportional, and integral gains are scaled to 0.094 and 7.573 respectively. At first, the desired output voltage value is compared with the output voltage measured from the load to acquire the corresponding voltage error. Then, it is fed to the PI controller to generate a reference current I_{ref}. Then, the reference current is compared with the actual inductor current to acquire the corresponding current error. Finally, this error is fed into the PWM generator to produce PWM pulses for controlling the duty ratio of the power switch S_2 to maintain the output voltage at 264 V.

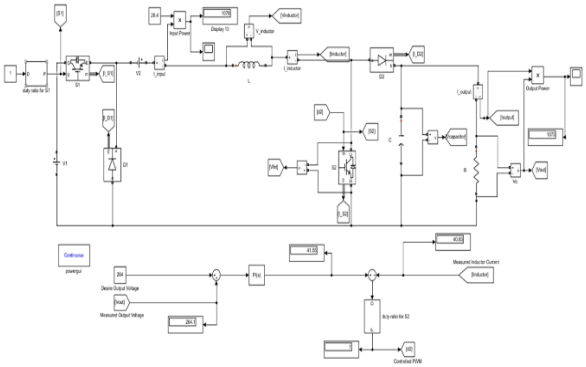

Fig. 10. Design of DIDCB converter with the implementation of control strategy 1.

Figure 11 illustrates the simulation waveform for the DIDCB converter when control strategy 1 is implemented. The time is scaled between 0.5 and 0.5005 seconds to show a clear image of the waveforms when switch S_2 is turned ON and OFF in short time intervals after the output voltage is stabilised. There is an overshoot in the inductor current before 0.05 seconds. After 0.15 seconds, it stabilises at 41.12 A. The output current increases and stabilises at 4.077 A after 0.041 seconds. Both the inductor and output current maintained their preferred values throughout the entire period of operation of the converter due to the constant regulation of control strategy 1. When power switch S_2 is turned ON, voltage sources S_1 and S_2 charge the inductor to 26.32 V. When power switch S_2 is turned OFF, the inductor discharges to – 239.05 V. The OFF duration of switch S_2 affects the discharge duration of the inductor voltage. The discharge duration is longer when switch S_2 is off for a longer time. This cycle is repeated until both switches are turned OFF.

Figure 12 shows the output voltage waveforms of the converter with a 65 Ω load resistance when the desired output voltage is set to different values. The simulation runs for 0.502 seconds. In Fig. 12(a), the output voltage overshoots to 56.96 V and stabilises at 50 V after 0.1 seconds. The output voltage of the converter increases and stabilises at 100 V without any overshoot, as shown in Fig. 12(b). Figure 12(c) depicts that the output voltage overshoots to 373.9 V but stabilises after 0.2 seconds at 263.7 V. This indicates the control strategy has the best performance in Fig. 12(b), where the desired output voltage and load resistance are 100 V and 65 Ω, respectively.

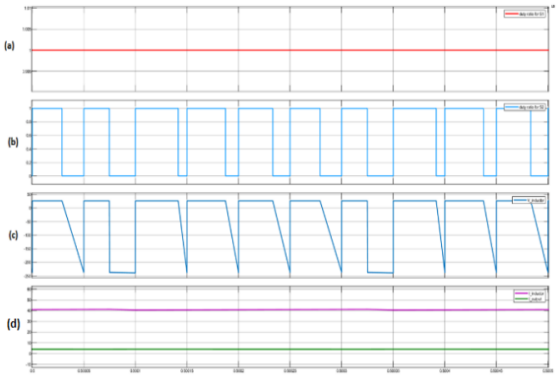

Fig. 11. Waveforms for DIDCB converter when converter strategy 1 is implemented with desired output set to 264 V. (a) Duty ratio $\boldsymbol{dS_1}$, (b) Duty ratio $\boldsymbol{dS_2}$, (c) Inductor voltage $\boldsymbol{V_L}$, (d) Inductor current $\boldsymbol{I_L}$ and output current $\boldsymbol{I_o}$.

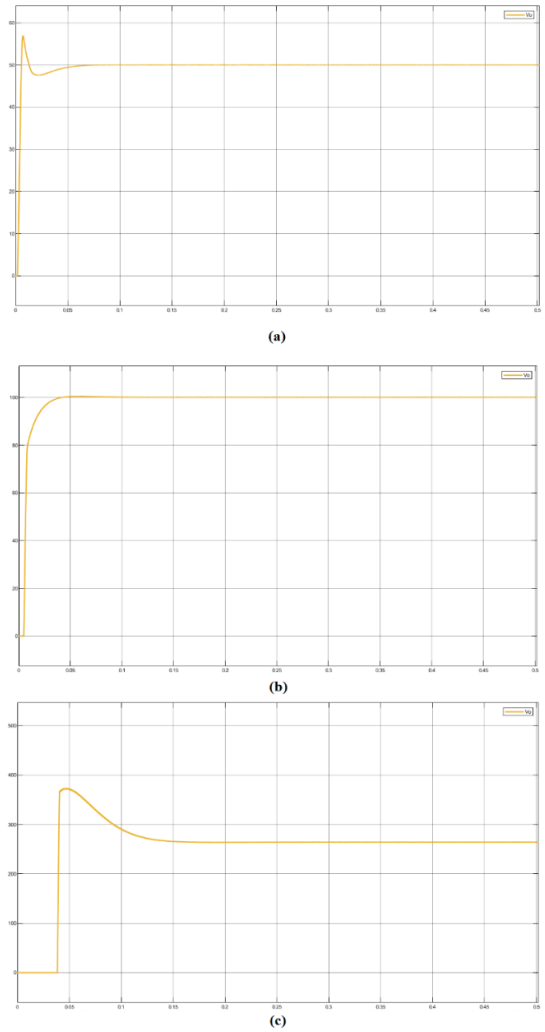

Fig. 12. Output voltage waveform for DIDCB converter when control strategy 1 is implemented with different desired output voltage set to: (a) 50 V (b) 100 V and (c) 264 V.

The simulated output voltage using different load variations is given in Fig. 13. The desired output voltage is set to 264 V. In Fig. 13(a), the output voltage of the converter is accompanied by a sharp spike before 0.05 seconds. The output voltage decreases and fluctuates continuously, even after 10 seconds have passed. This shows that control strategy 1 is incompatible with a load that has a low resistance. On the other hand, the output voltage in Fig. 13(b) has an overshoot at 359.1 V. However, it decreases quickly and stabilises at 0.25 seconds, with and the output voltage equals to 263.9 V. The parameters used for Fig. 13(c) are the same as Fig. 12(c). Hence, they have the same results. Figure 14 shows the output power of the converter with different load variations when duty ratios dS_1 and dS_2 are 1 and 0.9, respectively. It has similar waveforms to the ones in Fig. 13 as output power is affected by the output voltage. After stabilization, the output power for Fig. 14(b) and Fig. 14(c) is 1727 W and 1070 W, respectively.

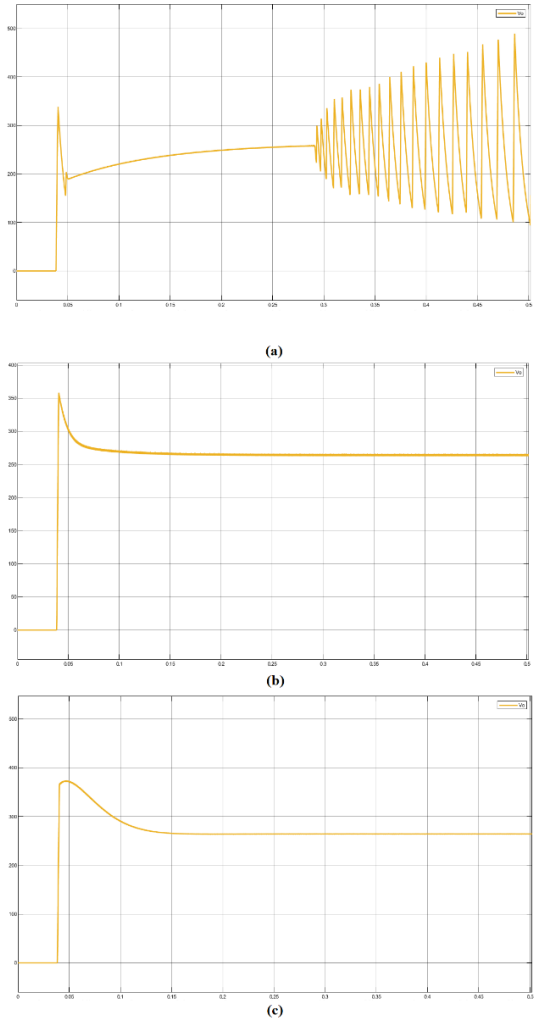

Fig. 13. Output voltage when control strategy 1 is implemented with different load variations at: (a) 20 Ω (b) 40 Ω and (c) 65 Ω.

Simulation results performed on a converter designed with control strategy 2 are shown in Fig. 15. The duty ratio dS_2 for power switch S_2 is modulated by the control strategy for output voltage regulation. The desired output is set to 264 V. The proportional and integral gains for the outer loop controller are scaled to 0.094 and 7.573 respectively. On the other hand, the proportional and integral gains for the inner loop controller are adjusted to 0.102 and 0.863, respectively. The saturation block limits the duty cycle of switch S_2 between 0.1 and 0.9 to reduce the overshoot of the output voltage. Initially, the desired

output voltage value is compared with the output voltage measured from the load to acquire the corresponding voltage error. The error is fed into the PI controller, which outputs the reference current I_{ref}. Then, it is compared with the measured inductor current value to obtain the corresponding current error. Another PI controller tunes the current error before passing it to a saturation block. Finally, pulses are produced by the PWM generator based on the output from the saturation block to control the duty ratio of the power switch S_2 so that the output voltage is maintained at 264 V.

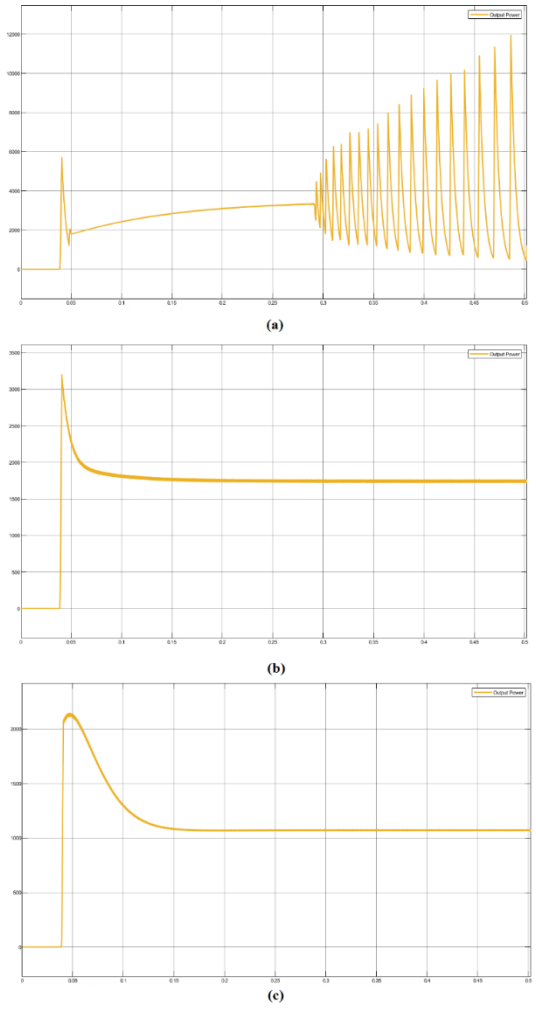

Fig. 14. Output power when control strategy 1 is implemented with different load variations at: (a) 20 Ω, (b) 40 Ω and (c) 65 Ω.

Figure 16 illustrates the simulation waveforms for the DIDCB converter when control strategy 2 is implemented. The time is scaled between 0.5 and 0.5005 seconds. The inductor current stabilises after 0.2 seconds at 40.4 A. On the other hand, the output current increases and stabilises at 4.035 A after 0.08 seconds. Both the inductor and output current maintained their preferred values throughout the entire operation period of the converter due to the constant regulation of control strategy 2. When power switch S_2 is turned ON, the voltage sources S_1 and S_2 charge the inductor to 26.32 V. When power switch S_2 is turned OFF for a short time, discharging of the inductor occurs with a voltage of –237.1 V. This cycle is repeated until both switches are turned OFF.

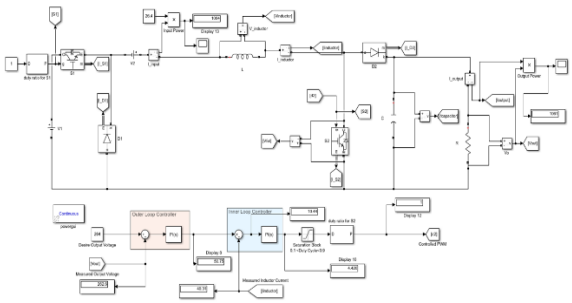

Fig. 15. Simulation Design of DIDCB Converter with the Implementation of Control Strategy 2.

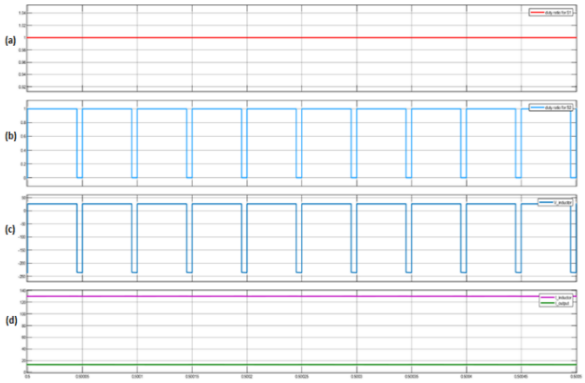

Fig. 16. Waveforms for DIDCB converter when control strategy 2 is implemented with desired output is set to 264 V. (a) Duty ratio $\boldsymbol{dS_1}$, (b) Duty ratio $\boldsymbol{dS_2}$, (c) Inductor voltage $\boldsymbol{V_L}$ and (d) Inductor current $\boldsymbol{I_L}$ and output current $\boldsymbol{I_o}$.

Figure 17 shows the output voltage waveforms when the desired output voltage is set to 50 V, 100 V, and 264 V, respectively, with load resistance equal to 65 Ω. Referring to Fig. 17(a), the output voltage of the converter has a sharp spike before 0.02 seconds. After 0.45 seconds, it stabilises at 50.3 V. Figure 17(b) shows that the output voltage increases and then stabilises at 100 V after 0.45 seconds. The output voltage in Fig. 17(c) increases to 278 V but quickly stabilises at 0.4 seconds at 262.3 V.

The simulated output voltage with different load variations is given in Fig. 18. The desired output voltage is set to 264 V. The output voltage of the converter in Fig. 18(a) is observed to have a few spikes occurring before 0.04 seconds. Then, it becomes steady at 261.2 V after 0.35 seconds. Figure 18(b) shows that the output voltage stabilises at 261.9 V after 0.3 seconds. The output voltage in Fig. 18(c) has the same settling time as Fig. 18(b). However, the output voltage stabilises at 262.6 V after an overshoot of 278 V at approximately 0.08 seconds. The contribution of power control strategy 2 is especially obvious at higher load resistances, as shown in Fig. 18(c). It is observed that the output voltage of the converter has fewer fluctuations, reduced overshoot, and a faster response time when compared to the output voltage waveform from the original design.

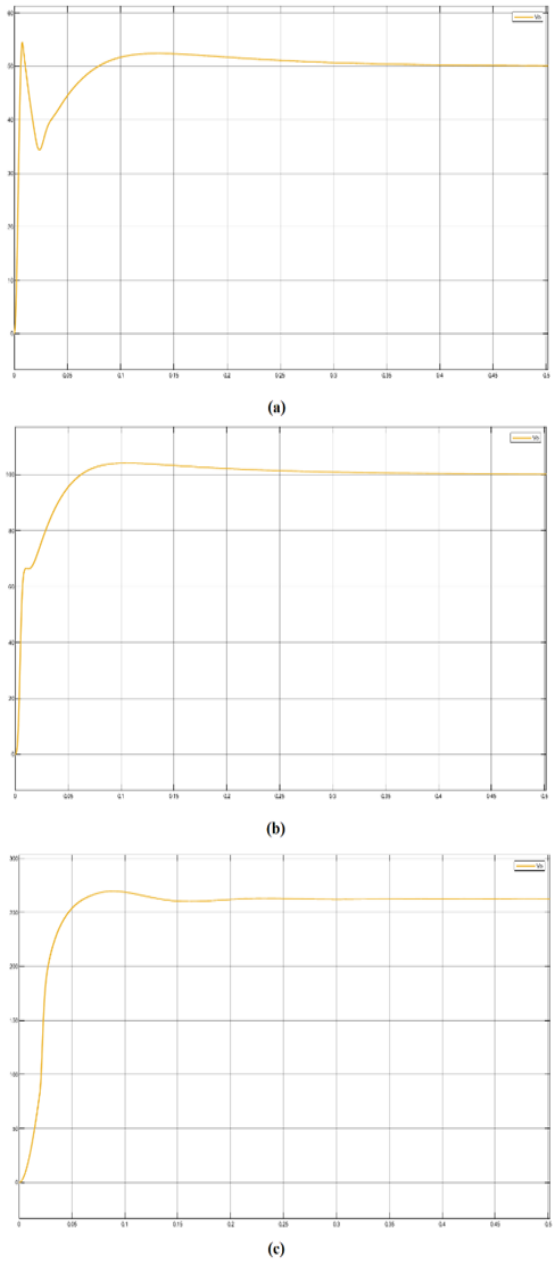

Fig. 17. Output voltage waveforms for DIDCB when control strategy 2 is implemented with different desired output voltage set to: (a) 50 V, (b) 100 V and (c) 264 V.

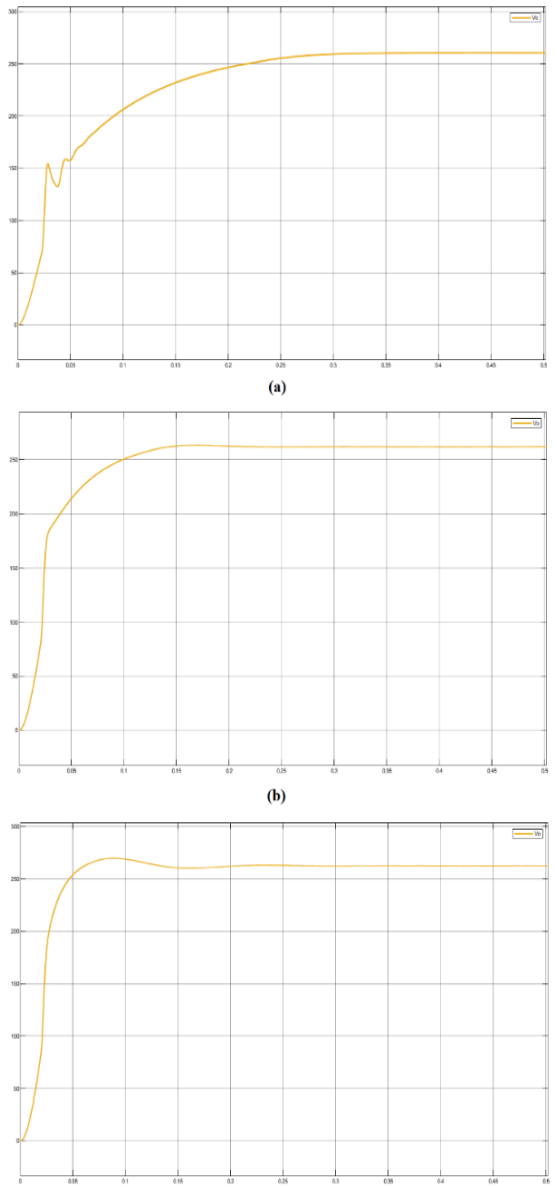

Fig. 18. Output voltage when control strategy 2 is implemented with different load variations at: (a) 20 Ω, (b) 40 Ω and (c) 65 Ω.

Figure 19 illustrates the output power of the converter with different load variations. It has similar waveforms to Fig. 18, as output power is affected by the output voltage. Despite that, the output voltage in Fig. 19(a) took a longer settling time and stabilised at 0.45 seconds at 3412 W. In Fig. 19(b), the output voltage increases and then stabilises at 1715 W after 0.3 seconds. On the other hand, the output voltage in Fig. 19(c) had an overshoot of 1037 W but quickly stabilised at 0.15 seconds at 1059.77 W.

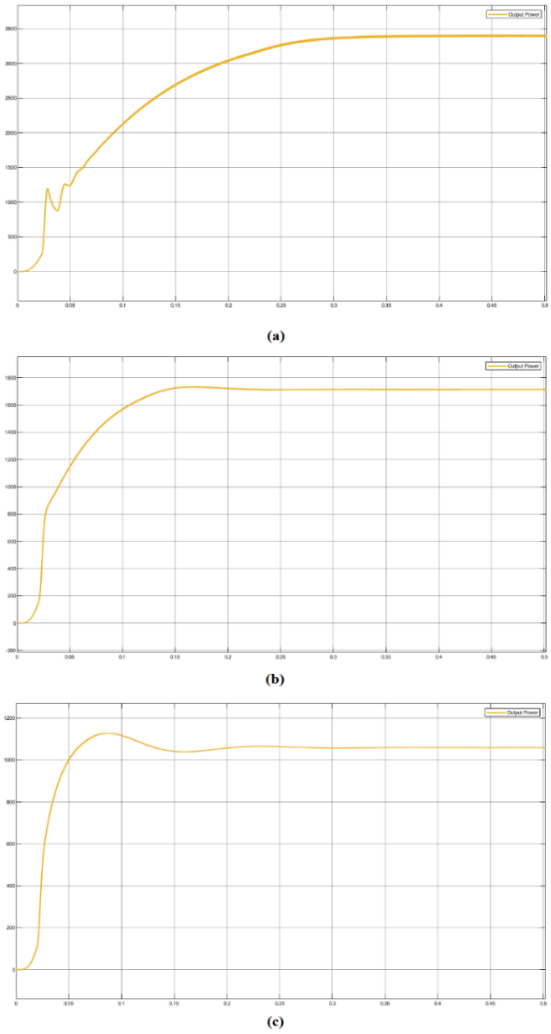

Fig. 19. Output power when control strategy 2 is implemented with different load variations at: (a) 20 Ω, (b) 40 Ω and (c) 65 Ω.

Table II shows the performance comparison between different DIDCB converter setups. The desired output voltage is set to 264 volts. The output voltage of the converter does not stabilise when power control strategy 1 is implemented with a 20 Ω load resistor. Hence, it is not listed in the table.

Based on Table II, the converter implemented with power control strategy 1 has the lowest efficiency among the three different set-ups. In addition, the control strategy 1 is also incompatible with loads that have low resistance. However, the output voltage waveform has lesser fluctuations, reduced overshoot, and higher efficiency when the proposed converter is implemented with power control strategy 2. Therefore, the power control strategy 2 is a more promising solution to regulate the output voltage of the proposed converter during load and source-side disturbances. In addition, it can be concluded that the efficiency of the converter increases as load resistance increases. This also means that the total output and input power of the converter will decrease as well.

Table III shows the comparison between the features of different MIDC converters. The output voltage and the efficiency of the proposed converter can be affected by the duty ratios dS_1 and dS_2 of the power switches. Hence, the DIDCB converter is observed to have a broad range of efficiency. However, the overall result still shows that the proposed converter can achieve higher efficiency, and lower active and passive components as compared to the other converters. The proposed converter also exhibited high voltage gain and low voltage stress using a simpler configuration and reduced size, contributing to a lower cost for the entire system design.

Table II: Comparison between the performance of the proposed converter with different set-ups.

Set-Up	Without Power Control Strategy			With Power Control Strategy 1		With Power Control Strategy 2		
Load Resistance R (Ω)	20	40	65	40	65	20	40	65
Output Voltage V_o (V)	261.20	261.90	262.60	263.90	263.70	261.20	261.90	262.60
Overshoot Percentage of Output Voltage (%)	-	11.04	30.26	-	41.79	-	-	3.20
Settling Time of Output Voltage (s)	0.35	0.35	0.40	0.25	0.20	0.35	0.30	0.30
Input Power P_{in} (W)	3438.00	1727.00	1066.03	1762.00	1078.00	3438.00	1727.00	1066.03
Output Power P_o (W)	3412.00	1715.00	1059.77	1727.00	1070.00	3412.00	1715.00	1059.77
Efficiency (%)	99.24	99.31	99.41	98.01	99.26	99.24	99.31	99.41

Table III: Comparison between features of different MIDC converters.

Topology Proposed	Number of Switch (Diode Included)	Number of Inductor	Number of Capacitor	Main Voltage Stress For Switch (V)	Operating Modes	Efficiency (%)
[4]	N+3	1	1	VN − VN−1	Bidirectional, Boost and Buckboost	76-88
[14]	N+3	2	4	VN	Unidirectional, Boost	76-90
[21]	N+4	1	1	VN	Bidirectional, Boost and Buckboost	84-93
[22]	N+3	1	1	VN	Unidirectional, Buckboost	85-95
[23]	2N+2	N	N+1	0.5VDS ID (ton +$toff$)+ 0.5$VDS2$ $Coss$	Bidirectional, Boost and Buck	94-97.5
[24]	11	3	5	Vo/2	Bidirectional, Boost	93-97
[25]	5	3	4	Vo	Unidirectional, Boost	88-94
Proposed converter	4	1	1	$V1$ +$V2$	Unidirectional, Boost	74.7-99.4

IV. CONCLUSION

A new design for a dual-input DC-DC boost converter is proposed. Current and voltage stress analyses have been performed to ensure suitable switching devices were selected for the converter. Two different power control strategies were proposed for the DIDCB converter to manage output voltage during source and load-side disturbances. The proposed design achieved a high efficiency of up to 99.4%. The performance of the converter is further improved with the implementation of a control strategy that results in less fluctuation in the output voltage waveform and reduced overshoot. Future work will consider using a PID controller as the control strategy to improve the stability of the system and modify the circuit to allow bidirectional power flow.

Lastly, the performance of the proposed converter will be verified through experimental realisation.

REFERENCES

[1] M. A. Bănică, "*Energy Harvesting from Renewable Energy Sources*," Cham: Springer International Publishing, pp. 247-254, 2019.

[2] J. F. Manwell, "*Hybrid Energy Systems*," Encyclopedia of Energy, C. J. Cleveland Ed., Elsevier, New York, pp. 215-229, 2004.

[3] A. Khaligh, C. Jian and L. Y. Joo, "A Multiple-Input DC-DC Converter Topology," *IEEE Trans. Power Electron.,* vol. 24, no. 3, pp. 862-868, 2009.

[4] A. Ponniran and A. Said, "DC-DC Boost Converter Design for Solar Electric System," *in Int. Conf. Instrument., Control., & Autom.*, Indonesia, pp. 210-214, 2009.

[5] F. Nejabatkhah, S. Danyali, S. H. Hosseini, M. Sabahi and S. M. Niapour, "Modeling and Control of a New Three-Input DC-DC Boost Converter for Hybrid PV/FC/Battery Power System," *IEEE Trans. Power Electron.,* vol. 27, no. 5, pp. 2309-2324, 2012.

[6] S. Danyali, S. H. Hosseini and G. B. Gharehpetian, "New Extendable Single-Stage Multi-input DC–DC/AC Boost Converter," *IEEE Trans. Power Electron.,* vol. 29, no. 2, pp. 775-788, 2014.

[7] S. Danyali, S. A. K. Mozaffari Niapour, S. H. Hosseini, G. B. Gharehpetian and M. Sabahi, "New Single-Stage Single-Phase Three-Input DC-AC Boost Converter for Stand-Alone Hybrid PV/FC/UC Systems," *Electric Power Sys. Res.,* vol. 127, pp. 1-12, 2015.

[8] A. Nahavandi, M. T. Hagh, M. B. B. Sharifian and S. Danyali, "A Nonisolated Multiinput Multioutput DC–DC Boost Converter for Electric Vehicle Applications," *IEEE Trans. Power Electron.,* vol. 30, no. 4, pp. 1818-1835, 2015.

[9] E. Babaei and O. Abbasi, "Structure for Multi-input Multi-output DC–DC Boost Converter," *IET Power Electron.,* vol. 9, no. 1, pp. 9-19, 2016.

[10] G. Chowdary, A. Singh and S. Chatterjee, "An 18 nA, 87% Efficient Solar, Vibration and RF Energy-Harvesting Power Management System with A Single Shared Inductor," *IEEE J. Solid-state Circuits,* vol. 51, no. 10, pp. 2501-2513, 2016.

[11] V. H. Garcia-Rodriguez, R. Silva-Ortigoza, E. Hernandez-Marquez, J. R. Garcia-Sanchez and H. Taud, "DC/DC Boost Converter-Inverter as Driver for A DC Motor: Modeling and Experimental Verification," *Energies,* vol. 11, no. 8, p. 2044, 2018.

[12] I. C. Chen, C. W. Liang and T. H. Tsai, "A Single-Inductor Dual-Input Dual-Output DC–DC Converter for Photovoltaic and Piezoelectric Energy Harvesting Systems," *IEEE Trans. Circ. and Sys. II: Express Briefs,* vol. 66, no. 10, pp. 1763-1767, 2019.

[13] P. Mohseni, S. H. Hosseini, M. Sabahi, T. Jalilzadeh and M. Maalandish, "A New High Step-Up Multi-Input Multi-Output DC–DC Converter," *IEEET Trans. Ind. Electron.,* vol. 66, no. 7, pp. 5197-5208, 2019.

[14] P. Mohseni, S. H. Hosseini, M. Sabahi and M. Maalandish, "A Multi-input Single-output High Step-up DC-DC Converter with Low-voltage Stress Across Semiconductors," *Int. Trans. Electr. Energy Sys.,* vol. 29, no. 12, e12123, 2019.

[15] Y. C. Hsu, J. Y. Lin, C. H. Wang and S. W. Chou, ‘‘An SIMO Stepdown Converter with Coupled Inductor,’’ *in Proc. Int. Symp. VLSI Design, Autom. Test*, pp. 1–4, 2020.

[16] Y. Zheng, J. Guo and K. N. Leung, ‘‘A Single-inductor Multiple-output Buck/boost DC–DC Converter with Duty-cycle and Control-current Predictor,’’ *IEEE Trans. Power Electron.*, vol. 35, no. 11, pp. 12022–12039, 2020.

[17] M. Y. Hassani, M. Maalandish and S. H. Hosseini, ‘‘A New Single-input Multi-output Interleaved High Step-up DC–DC Converter for Sustainable Energy Applications,’’ *IEEE Trans. Power Electron.*, vol. 36, no. 2, pp. 1544–1552, 2021.

[18] X. Zhang, B. Wang, X. Tan, H. B. Gooi, H. H. C. Iu and T. Fernando, ‘‘Deadbeat Control for Single-inductor Multiple-output DC–DC Converter with Effectively Reduced Cross Regulation,’’ *IEEE J. Emerg. Sel. Topics Power Electron.*, vol. 8, no. 4, pp. 3372–3381, 2020.

[19] H. Zhang, D. Dong, M. Jing W. Liu, and F. Zheng, ‘‘Topology Derivation of Multiple-port DC–DC Converters Based on Voltage-type Ports,’’ *IEEE Trans. Ind. Electron.*, vol. 69, no. 5, pp. 4742–4753, 2022.

[20] E. Durán, S. P. Litrán and M. B. Ferrera, ‘‘An interleaved Single-input Multiple-output DC–DC Converter Combination,’’ *CSEE J. Power Energy Sys.*, vol. 8, no. 1, pp. 132–142, 2022.

[21] S. Athikkal, K. Sundaramoorthy and A. Sankar, "Design, Fabrication and Performance Analysis of a Two Input-Single Output DC-DC Converter," *Energies*, vol.10, no. 9, 1410, 2017.

[22] S. Athikkal, K. Sundaramoorthy and A. Sankar, "Development and Performance Analysis of Dual-input DC–DC Converters for DC Microgrid Application," *IEEJ Trans. Electr. and Electron. Eng.*, vol. 13, no. 7, pp. 1034-1043, 2018.

[23] F. Akar, Y. Tavlasoglu and B. Vural, "Analysis and Experimental Verification of A Multi-input Converter for DC Microgrid Applications," *IET Power Electron.*, vol. 11, no. 6, pp. 1009-1017, 2018.

[24] S. H. Mirlohi, M. R. Yazdani, E. Adib and M. R. Amini, "Non-isolated High Step-up Dual-input DC-DC Converter with Zero-voltage Transition," *Int. J. Circuit Theory and Appl.*, vol. 48, no. 5, pp. 762-776, 2020.

[25] M. Foroughi and M. R. Amini, "A New Dual Input Boost Converter with Zero Voltage Switching," *Iran J. Sci. Technol. Trans. Electr. Eng.*, 45, pp. 415-423, 2021.